Biochemical Pharmacology 80 (2010) 1437–1449

Contents lists available at ScienceDirect

Biochemical Pharmacology

journal homepage: www.elsevier.com/locate/biochempharm

Comparison of the pharmacological properties of human and rat histamine H_3-receptors

David Schnell [a], Andrea Strasser [b], Roland Seifert [c,*]

[a] Department of Pharmacology and Toxicology, University of Regensburg, D-93040 Regensburg, Germany
[b] Department of Pharmaceutical/Medicinal Chemistry I, University of Regensburg, D-93040 Regensburg, Germany
[c] Institute of Pharmacology, Medical School of Hannover, Carl-Neuberg-Str. 1, D-30625 Hannover, Germany

ARTICLE INFO

Article history:
Received 18 May 2010
Received in revised form 20 July 2010
Accepted 23 July 2010

Keywords:
Active receptor state
Histamine H_3-receptor
Imoproxifan
Molecular dynamics simulations
Sf9 insect cells

ABSTRACT

Ligand pharmacology of histamine H_3-receptors is species-dependent. In previous studies, two amino acids in transmembrane domain 3 (TM III) were shown to play a significant role. In this study, we characterized human and rat histamine H_3-receptors (hH_3R and rH_3R, respectively), co-expressed with mammalian G proteins in Sf9 insect cell membranes. We compared a series of imidazole-containing H_3R ligands in radioligand binding and steady-state GTPase assays. H_3Rs similarly coupled to $G\alpha_{i/o}$-proteins. Affinities and potencies of the agonists histamine, N^{α}-methylhistamine and *R*-(α)-methylhistamine were in the same range. Imetit was only a partial agonist. The pharmacology of imetit and proxifan was similar at both species. However, impentamine was more potent and efficacious at rH_3R. The inverse agonists ciproxifan and thioperamide showed higher potency but lower efficacy at rH_3R. Clobenpropit was not species-selective. Strikingly, imoproxifan was almost full agonist at hH_3R, but an inverse agonist at rH_3R. Imoproxifan was docked into the binding pocket of inactive and active hH_3R- and rH_3R-models and molecular dynamic simulations were performed. Imoproxifan bound to hH_3R and rH_3R in *E*-configuration, which represents the *trans*-isomer of the oxime-moiety as determined in crystallization studies, and stabilized active hH_3R-, but inactive rH_3R-conformations. Large differences in electrostatic surfaces between TM III and TM V cause differential orientation of the oxime-moiety of imoproxifan, which then differently interacts with the rotamer toggle switch $Trp^{6.48}$ in TM VI. Collectively, the substantial species differences at H_3Rs are explained at a molecular level by the use of novel H_3R active-state models.

1. Introduction

Histamine (HA) exhibits its biological effects through the activation of four different G protein-coupled receptors (GPCRs). The histamine H_1-receptor (H_1R) is associated with inflammatory and allergic reactions, e.g. it increases vascular permeability and NO production [1]. The histamine H_2-receptor (H_2R) not only regulates gastric acid production, but also shows a positive inotropic effect on the heart [1]. The histamine H_3-receptor (H_3R) is a presynaptic auto- and heteroreceptor, regulating the release of HA and various other neurotransmitters in the nervous system, and is involved in important physiological processes like the sleep-wake cycle, eating behaviour and cognition [2]. The histamine H_4-receptor (H_4R) mediates inflammatory and immunological processes, e.g. chemotaxis of eosinophils, mast cells and dendritic cells, but it is also present on neurons mediating HA-induced itching [3,4]. H_1R and H_2R antagonists have been used as therapeutics for decades, H_3R and H_4R are still explored and promising new drug targets [5].

The H_3R was pharmacologically identified in the early 1980s, but cloned almost 20 years later in 1999 as an orphan GPCR [2]. The reason for this delay was that it only shares ~20% homology to the H_1R and H_2R. The complex gene structure of the human H_3R (hH_3R) gives rise to many possible splice variants. To date about 20 hH_3R splice variants are known [6], but their function still remains elusive. The H_3R displays high constitutive, i.e. ligand-independent, activity in many experimental systems [7]. The H_3R is one of the very few GPCRs for which constitutive activity has also been demonstrated *in vivo* [8].

For the H_3R it has also been shown that species-differences exist [9,10]. Fig. 1 shows the amino acid sequences of hH_3R and rH_3R. Although the H_3R sequence has a high degree of similarity among

Abbreviations: GPCR, G protein-coupled receptor; GTPγS, guanosine 5′-[γ-thio]triphosphate; h, human; r, rat; β_2AR, β_2-adrenoceptor; H_3R, histamine H_3-receptor; H_4R, histamine H_4-receptor; TM, transmembrane domain; JNJ-7753707, (4-fluorophenyl)(1-methyl-2-an-1*H*-imidazol-5-yl)methanone; FUB181, 4-(3-(3-(4-chlorophenyl)propoxy)propyl)-1*H*-imidazole; A-304121, (*R*)-2-amino-1-(4-(3-(4-(cyclopropanecarbonyl)phenoxy)-propyl)piperazin-1-yl)propan-1-one; fMLP, N-formyl-L-methionyl-L-leucyl-L-phenylalanine; THIO, thioperamide.

* Corresponding author. Tel.: +49 511 532 2805; fax: +49 511 532 4081.
E-mail address: seifert.roland@mh-hannover.de (R. Seifert).

0006-2952/$ – see front matter © 2010 Elsevier Inc. All rights reserved.
doi:10.1016/j.bcp.2010.07.027

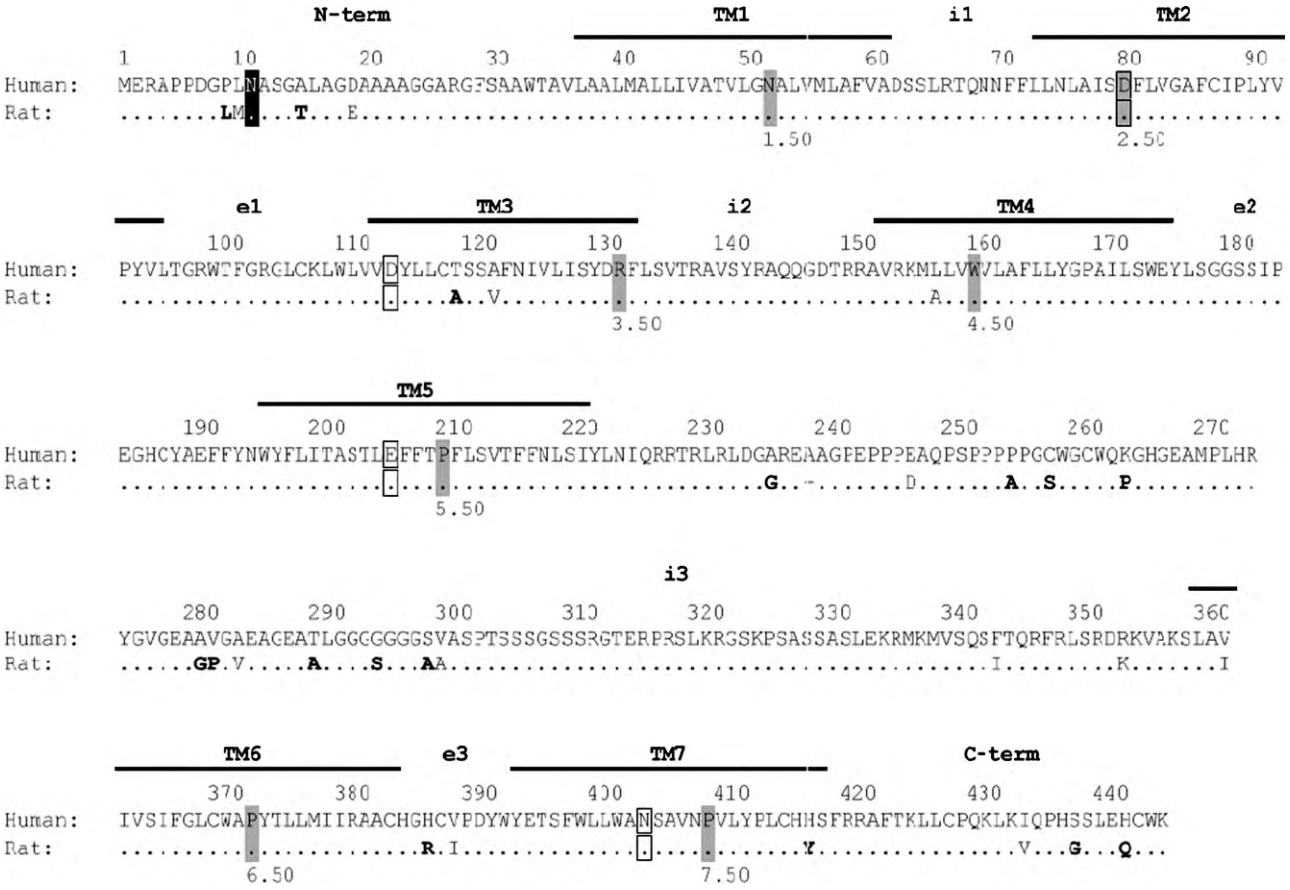

Fig. 1. Comparison of the amino acid sequences of hH_3R (GeneBank Accession No. AF140538) and rH_3R (GeneBank Accession No. AF237919). Putative transmembrane domains are stated above the sequences and indicated by a solid line. N-term, extracellular N-terminal domain of H_3Rs; C-term, intracellular C-terminal domain of H_3Rs; i1, i2, and i3, first, second, and third intracellular loops; e1, e2, e3, first, second, and third extracellular loops, respectively. Dots in the sequence of rH_3R indicate identity with hH_3R. Amino acids shown in regular fonts in the sequence of rH_3R represent conservative differences, those shown in bold represent non-conservative differences. The most conserved residues in each TM domain are indicated in grey shading. Residues within TM domains are named according to the Ballesteros/Weinstein nomenclature. The most conserved residue in each TM is numbered as *X*.50, where *X* is the number of the respective TM domain [11]. Amino acids shown in white with black shading represent a putative glycosylation site of the H_3R. Amino acids in frame represent putative interaction sites of HA with the H_3R [12,13].

species, differences located in key regions of the receptor protein account for differences in antagonist affinity [13,14]. Additionally, splice variants differ in composition and expression pattern between species, and there are potential differences in signal transduction processes between either tissues and/or species [15]. Nevertheless, there are still unresolved questions about species differences of the full-length and un-spliced H_3Rs (445 amino acids), especially regarding the detailed molecular mechanisms involved in ligand–receptor interactions.

In the present study, we systematically compared the pharmacological properties of hH_3R and rH_3R. Fig. 2 shows the structures of the compounds studied, all of them being imidazole-containing ligands. We co-expressed hH_3R and rH_3R in Sf9 cells together with mammalian G proteins in a defined stoichiometry, determined the affinity of ligands in radioligand binding studies, and their potency and efficacy in steady-state GTPase assays. The baculovirus/Sf9 cell system is very suitable for the analysis of G_i/G_o-coupled receptors and in particular constitutively active receptors, because in Sf9 cells no endogenous G_i/G_o-proteins or GPCRs with constitutive activity are present. The controlled expression of receptor and G proteins in Sf9 cell membranes represents more the physiological situation than, for example, the construction of GPCR-Gα fusion proteins, because fusion proteins do not exist physiologically and the mobility of the G proteins is not restricted in the co-expression system. Moreover, the use of very proximal read-outs, like radioligand binding or steady-state GTPase assays prevents possible bias in later steps of the signal transduction cascade.

Many studies of ligand–receptor interactions come to a point where structural information on the atomic level is needed to explain experimental results. In the case of GPCRs, this is a very challenging and time-consuming process, and at the end only snapshots of static ligand–receptor complexes are resolved [16]. However, more and more high-resolution crystal structures of inactive- and active-state GPCR–ligand complexes are becoming available and can be used to generate better homology models [17–19]. Several molecular modelling studies with regard to ligand–receptor interaction at H_3R are found in the literature [13,20–22]. Since active-state models for H_3Rs do not yet exist, we generated and used those models to explain the pharmacological species differences at hH_3R and rH_3R on the basis of experimental data.

2. Materials and methods

2.1. Materials

The cDNAs of the hH_3R and rH_3R were kindly provided by Dr. T. Lovenberg (Johnson & Johnson Pharmaceutical R&D, San Diego, CA, USA). An alignment of the corresponding amino acid sequences is given in Fig. 1. Anti-hH_3R Ig and anti-rH_3R Ig were from Bio-Trend (Cologne, Germany). The antibody recognizing both species homologs was from GeneWay (San Diego, CA, USA). All other

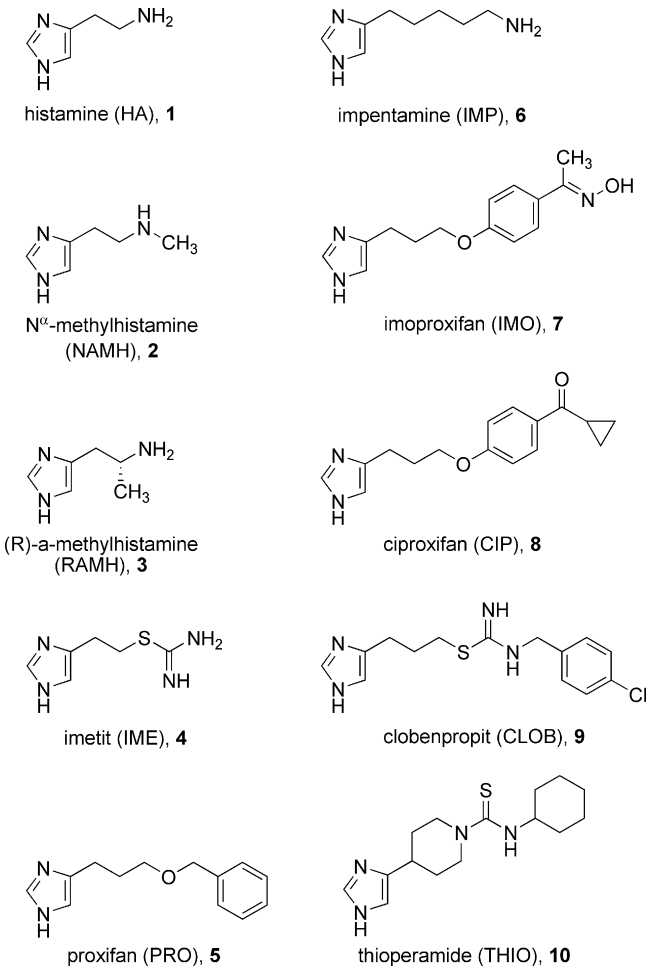

Fig. 2. Structures of imidazole-containing H_3R-ligands: full agonists (**1**–**3**), partial agonists (**4**–**6**), imoproxifan (**7**), and antagonists/inverse agonists (**8**–**10**).

antibodies, purified G proteins, reagents for molecular biology, recombinant baculoviruses encoding mammalian G protein subunits, and the sources of test compounds were described before [23]. Chemical structures of H_3R ligands are depicted in Fig. 2. Stock solutions (10 mM) of all H_3R ligands described in this paper were prepared in distilled water and stored at −20 °C. [^{3}H]JNJ-7753707 (=[^{3}H]RWJ-422475) (30 Ci/mmol) was kindly donated from Dr. P. Bonaventure (Johnson & Johnson Pharmaceutical R&D, San Diego, CA, USA). [^{3}H]N^{α}-methylhistamine (74–85 Ci/mmol) and [^{35}S]GTPγS (1100 Ci/mmol) were obtained from Perkin Elmer (Boston, MA, USA). [γ-^{32}P]GTP was synthesized as described [23]. Unlabeled nucleotides were from Roche (Indianapolis, IN, USA) and all other reagents were of the highest purity available and from standard suppliers.

2.2. Construction of FLAG epitope- and hexahistidine-tagged cDNAs for hH_3R and rH_3R

The cDNA for the tagged rH_3R protein was generated by sequential overlap-extension PCR in analogy to the procedure described recently for hH_3R [23]. In the case of rH_3R, the sense primer RAT HRH3-F (5′-GAC GAT GAT GAC GCC *ATG* GAG CGC GCG CCG CC-3′) consisted of 15 bp of the 3′-end of SF and the first 17 bp of the 5′-end of the rH_3R. The antisense primer RAT HRH3-RV (5′-GA TCC TCT AGA *TTA* GTG ATG GTG ATG ATG GTG CTT CCA GCA CTG CTC-3′) consisted of 15 bp of the C-terminus of the rH_3R, and encoded a hexahistidine tag, the *stop codon*, and a Xba I site. As template, a plasmid (pCIneo) containing the sequence of rH_3R was used.

2.3. Generation of recombinant baculoviruses, cell culture and membrane preparation, SDS-PAGE and immunoblot analysis

The protocols for virus amplification, protein expression and western blot analysis were described before [23]. Proteins transferred to nitrocellulose membranes were reacted with anti-hH_3R (N-term) (1:1000), anti-rH_3R (C-term) (1:1000) and anti-H_3R (i3) (1:1000) Igs.

2.4. [^{35}S]GTPγS saturation binding assay

Experiments were performed in analogy to the assay described in Schnell et al. [23]. Membranes were thawed and sedimented by a 10-min centrifugation at 4 °C and 15,000 × *g* to remove residual endogenous guanine nucleotides as far as possible. Membranes were resuspended in binding buffer (12.5 mM $MgCl_2$, 1 mM EDTA, and 75 mM Tris–HCl, pH 7.4), supplemented with 0.05% (m/v) BSA. Each tube (total volume of 250 or 500 μl) contained 10–20 μg of membrane protein. Tubes contained 0.2–2 nM [^{35}S]GTPγS plus unlabeled GTPγS to give the desired final ligand concentrations (0.2–50 nM). Neither GDP nor H_3R ligands were included in assays. Non-specific binding was determined in the presence of 100 μM unlabeled GTPγS and amounted to less than 1% of total binding. Incubations were conducted for 90 min at 25 °C and shaking at 250 rpm. Bound [^{35}S]GTPγS was separated from free [^{35}S]GTPγS by filtration through GF/C filters, followed by three washes with 2 ml of binding buffer (4 °C). Filter-bound radioactivity was determined by liquid scintillation counting. The experimental conditions chosen ensured that not more than 10% of the total amount of radioactivity added to binding tubes was bound to filters. The maximum number of $G\alpha_{i/o}$-related GTPγS binding sites in membranes expressing H_3Rs plus Gα-subunits plus $\beta_1\gamma_2$ was corrected by the binding determined in parallel in membranes expressing H_3Rs plus $\beta_1\gamma_2$ alone. These reference membranes were always prepared under exactly the same conditions as the other ones. To ensure the same viral load in the reference membranes, Sf9 cells were infected with baculoviruses encoding H_3Rs, $\beta_1\gamma_2$ and virus encoding no recombinant protein at all. In this manner, only the number of functionally intact and heterologously expressed mammalian $G\alpha_{i/o}$-subunits was quantitated.

2.5. Steady-state GTPase activity assay

Experiments were performed in analogy to the assay described in Schnell et al. [23]. Briefly, membranes were thawed, sedimented and resuspended in 10 mM Tris/HCl, pH 7.4. Assay tubes contained Sf9 membranes (10–20 μg of protein/tube), 5.0 mM $MgCl_2$, 0.1 mM EDTA, 0.1 mM ATP, 100 nM GTP, 0.1 mM adenylyl imidodiphosphate, 1.2 mM creatine phosphate, 1 μg of creatine kinase, and 0.2% (w/v) bovine serum albumin in 50 mM Tris/HCl, pH 7.4, and H_3R ligands at various concentrations. Reaction mixtures (80 μl) were incubated for 2 min at 25 °C before the addition of 20 μl of [γ-^{32}P]GTP (0.1 μCi/tube). All stock and work dilutions of [γ-^{32}P]GTP were prepared in 20 mM Tris/HCl, pH 7.4. Reactions were conducted for 20 min at 25 °C. Reactions were terminated by the addition of 900 μl of slurry consisting of 5% (w/v) activated charcoal and 50 mM NaH_2PO_4, pH 2.0. Charcoal absorbs nucleotides but not P_i. Charcoal-quenched reaction mixtures were centrifuged for 7 min at room temperature at 15,000 × *g*. Six hundred microliters of the supernatant fluid of reaction mixtures were removed, and $^{32}P_i$ was determined by liquid scintillation counting. Enzyme activities were corrected for spontaneous degradation of [γ-^{32}P]GTP. Spontaneous [γ-^{32}P]GTP degradation was determined in tubes containing all of the above described components plus a very high concentration of unlabeled GTP (1 mM) that, by competition with [γ-^{32}P]GTP, prevents

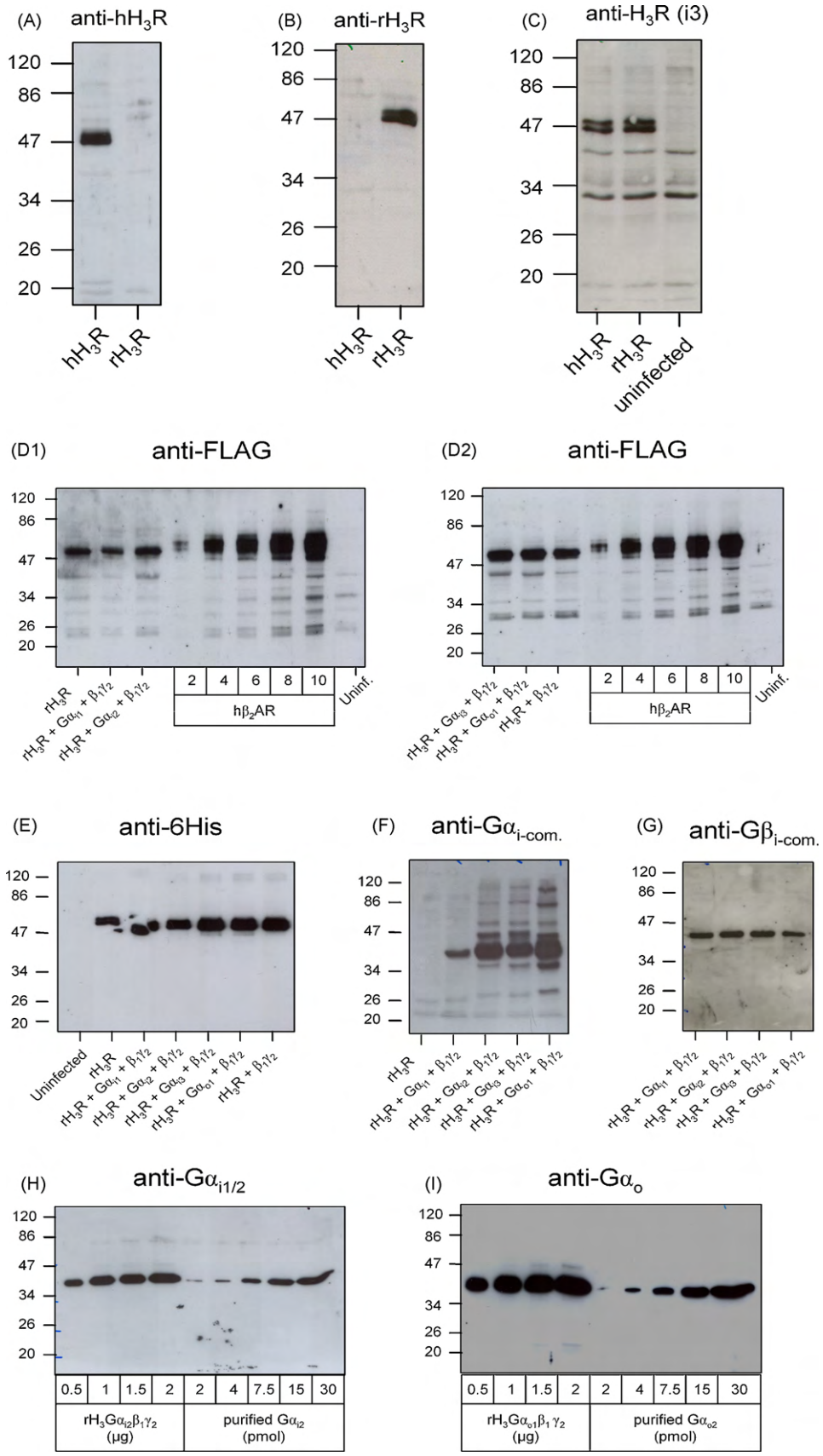

Fig. 3. Immunological detection of hH_3R and rH_3R expressed in Sf9 cells. Each lane of the gels was loaded with 10 μg of membrane protein, unless otherwise indicated below the film. Numbers on the left designate masses of marker proteins in kDa. In (A) and (B), membranes expressing the hH_3R and rH_3R alone were loaded onto the gels. Proteins separated in (A) were reacted with anti-hH_3R Ig and in (B) with anti-rH_3R Ig. In (C), membranes of (A) and (B) plus control were analyzed. Here, the proteins were reacted with the non-species-selective anti-hH_3R (i3) Ig. In (D1) and (D2), 2, 4, 6, 8 and 10 μg of protein of Sf9 membranes expressing $h\beta_2AR$ at 7.5 pmol/mg (as determined by [^{3}H]dihydroalprenolol saturation binding) were used as standard to assess the expression levels of the rH_3R in different membrane preparations with anti-FLAG Ig. In (E), the

[γ-^{32}P]GTP hydrolysis by enzymatic activities present in Sf9 membranes. Spontaneous [γ-^{32}P]GTP degradation was <1% of the total amount of radioactivity added using 20 mM Tris/HCl, pH 7.4, as solvent for [γ-^{32}P]GTP. The experimental conditions chosen ensured that not more than 10% of the total amount of [γ-^{32}P]GTP added was converted to $^{32}P_i$.

2.6. Radioligand binding assays

Experiments were performed in analogy to the assay described in Schnell et al. [23]. Membranes were thawed and sedimented by a 10-min centrifugation at 4 °C and 15,000 × *g* and resuspended in binding buffer (12.5 mM $MgCl_2$, 1 mM EDTA, and 75 mM Tris–HCl, pH 7.4), to remove residual endogenous guanine nucleotides as much as possible. In [^{3}H]NAMH binding assays, each tube (total volume, 250 or 500 μl) contained 10–50 μg of protein. Non-specific binding was determined in the presence of [^{3}H]NAMH at various concentrations plus 10 μM THIO and amounted to ~10% of total binding at saturating concentrations (10 nM). Incubations were conducted for 60 min at RT and shaking at 250 rpm. Saturation binding experiments were carried out using 0.3–10 nM [^{3}H]NAMH in the presence or absence of 10 μM GTPγS. In competition binding experiments, tubes contained 1 nM [^{3}H]NAMH and unlabeled ligands at various concentrations. Bound [^{3}H]NAMH was separated from free [^{3}H]NAMH by filtration through GF/C filters pretreated with 0.3% (m/v) polyethyleneimine, followed by three washes with 2 ml of binding buffer (4 °C). [^{3}H]JNJ-7753707 (=[^{3}H]RWJ-422475) binding experiments were performed using the same procedure as described above for [^{3}H]NAMH. With [^{3}H]JNJ-7753707 as radioligand, non-specific binding was about 20–30% of total binding at saturating concentrations (10 nM). Filter-bound radioactivity was determined by liquid scintillation counting. The experimental conditions chosen ensured that not more than 10% of the total amount of radioactivity added to binding tubes was bound to filters.

2.7. Construction of inactive and active models of hH_3R and rH_3R

Based on the crystal structure of the human β_2-adrenergic receptor [17,24], a homology model of the inactive hH_3R and rH_3R were generated. Based on the active state model of guinea pig H_1R (gpH_1R) [25,26], an active model of hH_3R was constructed by homology modelling. All models were refined and energetically minimized with SYBYL 7.0 (Tripos, St. Louis, MO, USA), as described [27]. Imoproxifan was docked manually into the binding pocket of the active hH_3R and the inactive rH_3R. Thereby, previous results of similar compounds were taken into account [20,21]. The resulting structures were embedded in a simulation box, including lipid bilayer, water, sodium and chlorine ions, as described [28]. Subsequently, molecular dynamic simulations with GROMACS 3.3.1 [29] were performed, using a simulation protocol, previously described [28].

2.8. Miscellaneous

Molecular biology was planned with GCK 2.5 (Textco BioSoftware, West Lebanon, NH, USA). Ligand structures were illustrated using ChemDraw Ultra 8.0 (CambridgeSoft, Cambridge, MA, USA). The sequence alignment was performed using Clustal X (2.0), which is a windows interface based on the Clustal W algorithm [30]. Protein was determined using the DC protein assay kit (Bio-Rad, Hercules, CA, USA). [^{3}H]Dihydroalprenolol was obtained from Perkin Elmer (Boston, MA, USA) and protein quantification via western blot performed as described in Schnell et al. [23]. All analyses of experimental data were performed with the Prism 5 program (GraphPad Software, San Diego, CA, USA).

3. Results

3.1. Western blot analysis of hH_3R and rH_3R expressed in Sf9 insect cell membranes

Membranes of Sf9 cells expressing hH_3R or rH_3R plus mammalian G proteins were prepared and analyzed via immunoblot. It has to be mentioned, that membranes co-expressing rH_3R plus different mammalian G proteins were prepared in parallel and under exactly the same conditions as the membranes expressing hH_3R [23]. Thus, the comparison of hH_3R and rH_3R pharmacology in this system is not based on historical data but direct. Both hH_3R and rH_3R bands were doublets, probably representing differently glycosylated forms (Fig. 3). H_3R species homologs presumably exhibit similar glycosylation patterns since the putative N-glycosylation site for the H_3R (Asn11) is fully conserved within their sequences (Fig. 1). The H_3R species homologs could be clearly discriminated by anti-hH_3R Ig, raised against an 18 amino acid peptide within the extracellular N-terminus of the hH_3R, and anti-rH_3R Ig, raised against an 18 amino acid peptide within the cytoplasmatic C-terminus of the rH_3R (Fig. 3A and B). Additionally, anti-H_3R (i3) Ig was used to confirm the above mentioned results (Fig. 3C). This antibody was raised against a peptide sequence within the third intracellular loop (i3) of the hH_3R, but turned out to be not species-selective. Again, all H_3R bands occurred as doublets at ~49 kDa. However, there were some additional bands at lower molecular weight, which are presumably non-specific, since they also appeared at the control lane loaded with uninfected Sf9 cell membranes. Thus, our data indicate that hH_3R and rH_3R were equally well and properly expressed in Sf9 cells. In analogy to our recent publication [23], the rH_3R was also co-expressed with different mammalian G proteins ($G\alpha_{i1}$, $G\alpha_{i2}$, $G\alpha_{i3}$ or $G\alpha_{o1}$, and $\beta_1\gamma_2$ dimers, respectively) to analyze the coupling profile. All proteins were properly detected by different selective antibodies (Fig. 3). Moreover, we also quantified the expression levels of receptors and G proteins by immunoblot, using $h\beta_2AR$ or purified G protein subunits as standards (Fig. 3D, H, and I). The results of these studies are summarized in Table 1.

3.2. Quantitative analysis of receptor-to-G protein stoichiometries

Protein quantification via western blot is semi-quantitative and does not discriminate between functional and non-functional proteins. Therefore, we directly used a recently described combination of antagonist [^{3}H]JNJ-7753707- and [^{35}S]GTPγS-saturation binding [23] and calculated the functional GPCR/Gα protein ratios (Table 1). Similar to the membranes expressing hH_3R, we detected an excess of mammalian G proteins in the case of rH_3R, confirming the previously reported results [23]. Thus, G protein expression level is not limiting in this experimental system, too.

3.3. hH_3R and rH_3R coupling to different Gα-subunits

The G protein coupling profile of rH_3R (Table 2) was also investigated as for the hH_3R [23]. Briefly, receptor-dependent [γ-^{32}P]GTP hydrolysis of different Gα-subunits was measured

same membranes were reacted with anti-His6 Ig. In (F), the membranes were reacted with anti-$G\alpha_{i\text{-common}}$ Ig. In (G), the membranes were reacted with anti-$G_{\beta\text{-common}}$ Ig. In (H), 0.5, 1.0, 1.5 and 2.0 μg of a membrane expressing the $rH_3R + G\alpha_{i2} + \beta_1\gamma_2$ was analyzed in order to quantify the Gα-subunits, using 2, 4, 7.5, 15 and 30 pmol of purified $G\alpha_{i2}$ as standard. In (I), 0.5, 1.0, 1.5 and 2.0 μg of a corresponding membrane of the same batch expressing $rH_3R + G\alpha_{o1} + \beta_1\gamma_2$ was analyzed to quantify the Gα-subunits, using 2, 4, 7.5, 15 and 30 pmol of purified $G\alpha_{o2}$ an almost identical splice variant of $G\alpha_{o1}$ as standard.

Table 1
Quantification of rH_3R-to-G protein ratios via western blot, [^{3}H]JNJ-7753707- and [^{35}S]GTPγS-saturation binding.

Membrane	$rH_3R + \beta_1\gamma_2$			
	$+G\alpha_{i1}$	$+G\alpha_{i2}$	$+G\alpha_{i3}$	$+G\alpha_{o1}$
$B_{max} \pm$ S.E.M. (pmol × mg^{-1})				
Immunoblot: anti-FLAG Ig	~1.5–2.5	~1.5–2.5	~1.5–2.5	~1.5–2.5
Anti-Gα Igs	n.d.	~50–100	n.d.	~50–100
[^{3}H]JNJ-7753707	0.67 ± 0.03	0.77 ± 0.02	1.05 ± 0.04	1.25 ± 0.04
[^{35}S]GTPγS	3.40 ± 0.80	4.43 ± 0.53	2.52 ± 0.37	8.19 ± 1.27
R:G ratio	~1:5	~1:6	~1:2	~1:7

The quantification of receptors and G proteins via immunoblot was performed as described [23]. [^{3}H]JNJ-7753707 saturation bindings were performed as described under Section 2. [^{35}S]GTPγS saturation bindings were performed, using Sf9 cell membranes from the same batch of preparation. Reaction mixtures contained membranes (10–20 μg of protein), 0.2–2 nM of [^{35}S]GTPγS, and unlabeled GTPγS to give the desired final ligand concentrations for saturation (0.2–50 nM). GDP or additional H_3R ligands were not present in the reaction mixtures. Data were analyzed by nonlinear regression and were best fitted to hyperbolic one-site saturation isotherms. The maximal number of GTPγS binding sites in membranes expressing rH_3R plus $G\alpha_{i2}$ plus $\beta_1\gamma_2$ was corrected by the binding determined in rH_3R plus $\beta_1\gamma_2$. By this way, the number of functionally intact and heterologously expressed G protein α-subunits was quantified. Data shown are the means ± S.E.M. of 3 independent experiments performed in triplicate. Receptor-to-G protein ratios were calculated, using the B_{max} values determined for the different membrane preparations.

Table 2
Analysis of rH_3R/G protein coupling – GTPase activities in Sf9 membranes expressing rH_3R and different $G\alpha_{i/o}$-proteins.

GTPase activity ± S.E.M.	$rH_3R + \beta_1\gamma_2$			
	$+G\alpha_{i1}$	$+G\alpha_{i2}$	$+G\alpha_{i3}$	$+G\alpha_{o1}$
Basal (pmol × mg^{-1} × min^{-1})	1.22 ± 0.21	1.75 ± 0.22	1.12 ± 0.04	4.29 ± 0.12
+Ago. (pmol × mg^{-1} × min^{-1})	2.01 ± 0.26	3.17 ± 0.37	2.13 ± 0.14	5.95 ± 0.14
ΔAgo. (pmol × mg^{-1} × min^{-1})	0.79 ± 0.07	1.42 ± 0.15	1.01 ± 0.10	1.66 ± 0.09
Agonist stimulation (% of basal)	67.44 ± 0.09	81.78 ± 2.32	89.38 ± 5.14	38.78 ± 2.38
+Inv. ago. (pmol × mg^{-1} × min^{-1})	0.71 ± 0.10	0.85 ± 0.12	0.59 ± 0.03	2.86 ± 0.14
ΔInv. ago. (pmol × mg^{-1} × min^{-1})	0.51 ± 0.13	0.90 ± 0.10	0.53 ± 0.02	1.43 ± 0.13
Inverse agonist inhibition (% of basal)	40.32 ± 5.93	51.66 ± 0.96	47.4 ± 0.82	33.29 ± 2.88

Steady-state GTPase experiments were performed as described in Section 2. Reaction mixtures contained 0.1 μCi [γ-^{32}P]GTP and 100 nM unlabeled GTP in the presence of solvent (basal), 10 μM HA (+ago.) or 10 μM THIO (+inv. ago.). Data shown are the means ± S.E.M. of three to four independent experiments for each membrane preparation performed in duplicates. The absolute agonist-stimulation (Δago.) and inverse agonist-inhibition (Δinv. ago.) of GTP hydrolysis, as well as the relative agonist-stimulation and inverse agonist-inhibition of GTP hydrolysis (% of basal), were calculated.

under steady-state conditions. GTPase activities were determined in parallel under basal conditions, maximal stimulation with the physiological (and full) agonist histamine (10 μM) and a saturating concentration of the inverse agonist thioperamide (10 μM) in Sf9 cell membranes co-expressing the rH_3R and different G proteins.

Like hH_3R, rH_3R coupled efficiently to all co-expressed mammalian $G\alpha_{i/o}$-subunits ($G\alpha_{i1}$, $G\alpha_{i2}$, $G\alpha_{i3}$ or $G\alpha_{o1}$, and $\beta_1\gamma_2$ dimers, respectively), as was evident by the high basal GTPase activities and the large absolute stimulatory and inhibitory effects of histamine and thioperamide, respectively (Table 2). Also, the relative stimulatory effects of histamine and the relative inhibitory effects of thioperamide based on total ligand-regulated GTPase activity were similar for each of the four systems studied, indicating that the constitutive activity of rH_3R was comparable and not substantially influenced by the type of G protein (Table 2). The constitutive activity of rH_3R coupled to cognate G_i/G_o-proteins was rather high and comparable to the constitutive activity of hH_3R, rendering the two systems suitable for an analysis of species-specific ligand effects, without possible bias due to differences in basal activity between membranes.

3.4. Ligand potencies and efficacies in the steady-state GTPase assay at rH_3R compared to hH_3R co-expressed with different Gα-subunits

Next, we examined a series of imidazole-based ligands in Sf9 cell membranes expressing rH_3R and different $G\alpha_{i/o}$-proteins in the steady-state GTPase assay. The data (Table 3) were then compared with the results for hH_3R [23] (Fig. 4A and B). The endogenous agonist histamine (**1**) and the standard H_3R ligands N^{α}-methylhistamine (**2**) and (*R*)-α-methylhistamine (**3**) were full agonists and equally potent in all membranes. There were essentially no species-differences. The highly potent standard H_3R agonist imetit (**4**) was almost a full agonist at rH_3R, too. Interestingly, proxifan (**5**) was again a strong partial agonist in all systems, independent of the G protein subtype co-expressed, corroborating the notion that this ligand does not show functional selectivity at H_3Rs [23]. In contrast to hH_3R, impentamine (**6**) was a strong and more potent partial agonist at rH_3R in all experimental settings. Strikingly, imoproxifan (**7**) was an almost full agonist at hH_3R (Fig. 5A), but an inverse agonist at rH_3R (Fig. 5B). The type of G protein subunit did not change the pharmacological profile of imoproxifan (Table 3). The inverse agonists ciproxifan (**8**) and thioperamide (**10**) were more potent but less efficacious at rH_3R than at hH_3R and again, the G protein subtype caused no changes in their profiles. Clobenpropit (**9**) was neither species-specific nor did the G protein subtype change its pharmacology. Moreover, there is also a strong linear correlation between potencies and efficacies of imidazole-based ligands at membranes expressing rH_3R and different $G\alpha_{i/o}$-subunits, as was found for the hH_3R (Fig. 6 and Table 3). Thus, the pharmacological profile of the rH_3R is also very similar under the various experimental conditions and, like at hH_3R, ligand-specific receptor conformations leading to coupling differences do not exist for the compounds investigated [23].

Collectively, these results confirm the findings regarding the relative stimulatory and inhibitory effects of histamine and thioperamide, respectively (Table 2), based on total ligand-regulated GTPase activity and are indicative for similar constitutive activity of hH_3R and rH_3R under all experimental conditions. If there had been differences in constitutive activity between hH_3R and rH_3R, then systematic changes in the potencies of full agonists

Table 3
Ligand potencies and efficacies in the GTPase assay at Sf9 cell membranes expressing the rH_3R and different G proteins.

	$rH_3R + G\alpha_{i1} + \beta_1\gamma_2$		$rH_3R + G\alpha_{i2} + \beta_1\gamma_2$		$rH_3R + G\alpha_{i3} + \beta_1\gamma_2$		$rH_3R + G\alpha_{o1} + \beta_1\gamma_2$	
	$pEC_{50} \pm$ S.E.M.	$E_{max} \pm$ S.E.M.	$pEC_{50} \pm$ S.E.M.	$E_{max} \pm$ S.E.M.	$pEC_{50} \pm$ S.E.M.	$E_{max} \pm$ S.E.M.	$pEC_{50} \pm$ S.E.M.	$E_{max} \pm$ S.E.M.
HA	$7.64 \pm 0.07^{*}$	1.00	7.94 ± 0.05	1.00	7.88 ± 0.06	1.00	7.72 ± 0.05	1.00
NAMH	8.30 ± 0.23	0.91 ± 0.10	8.98 ± 0.12	1.06 ± 0.07	9.11 ± 0.30	1.16 ± 0.21	8.88 ± 0.18	1.10 ± 0.11
RAMH	8.06 ± 0.17	0.88 ± 7.14	8.54 ± 0.10	0.91 ± 0.05	8.50 ± 0.08	0.90 ± 0.03	8.21 ± 0.10	0.84 ± 0.04
IME	9.86 ± 0.19	0.95 ± 0.10	9.76 ± 0.13	0.89 ± 0.06	10.14 ± 0.36	1.39 ± 0.30	9.78 ± 0.12	0.99 ± 0.07
PRO	8.12 ± 0.22	0.48 ± 0.05	8.52 ± 0.12	0.66 ± 0.04	8.42 ± 0.10	0.64 ± 0.04	8.19 ± 0.16	0.66 ± 0.05
IMP	8.33 ± 0.15	0.72 ± 0.05	8.94 ± 0.20	0.91 ± 0.10	8.99 ± 0.26	0.95 ± 0.14	8.76 ± 0.12	0.84 ± 0.06
IMO	9.03 ± 0.26	-0.61 ± 0.08	9.03 ± 0.13	-0.61 ± 0.04	9.05 ± 0.23	-0.46 ± 0.05	8.93 ± 0.16	$-0.96 \pm 0.08^{**}$
CIP	8.71 ± 0.27	-0.81 ± 0.10	8.64 ± 0.10	-0.75 ± 0.03	8.64 ± 0.15	-0.61 ± 0.04	8.58 ± 0.16	-1.01 ± 0.07
CLOB	9.04 ± 0.26	-0.43 ± 0.05	8.95 ± 0.16	-0.44 ± 0.03	8.77 ± 0.13	-0.41 ± 0.02	8.68 ± 0.11	$-0.69 \pm 0.03^{**}$
THIO	7.82 ± 0.24	-0.66 ± 0.07	7.66 ± 0.12	-0.62 ± 0.03	7.61 ± 0.13	-0.50 ± 0.03	7.64 ± 0.08	$-0.99 \pm 0.03^{***}$
r^2	0.77	0.99	1.00	1.00	0.97	0.96	0.96	0.996
Slope	0.99 ± 0.19	0.97 ± 0.04	1.00	1.00	1.17 ± 0.07	0.99 ± 0.07	1.05 ± 0.07	1.20 ± 0.03

Steady-state GTPase activity in Sf9 membranes expressing rH_3R, different $G\alpha_{i/o}$ subunits and $\beta_1\gamma_2$ was determined as described under Section 2. Reaction mixtures contained ligands at concentrations from 0.1 nM to 10 μM as appropriate to generate saturated concentration/response curves. Data were analyzed by nonlinear regression and were best fit to sigmoid concentration/response curves. Typical basal GTPase activities ranged between 1.0 and 4.0 pmol × mg^{-1} × min^{-1}, and the maximal stimulatory effect of histamine (10 μM) amounted to ~40 to ~90% above basal. The efficacy (E_{max}) of histamine was determined by nonlinear regression and was set to 1.00. The E_{max} values of other agonists and inverse agonists were referred to this value. Data shown are the means ± S.E.M. of three to four experiments performed in duplicates each. Statistical analysis was performed using one-way ANOVA, followed by Dunnet's multiple comparison test using the values determined at hH_3R, $G\alpha_{i2}$ and $\beta_1\gamma_2$ as a reference. Significant differences to the membrane expressing $G\alpha_{i2}$ are shown following comparison with other $G\alpha_{i/o}$ subunits. Additionally, data shown were correlated and analyzed by linear regression. The potencies and efficacies of ligands at membranes co-expressing the rH_3R, $G\alpha_{i1}$, $G\alpha_{i3}$ or $G\alpha_{o1}$, and $\beta_1\gamma_2$ dimers, respectively, were correlated with values determined at the reference membrane expressing $G\alpha_{i2}$. The correlation coefficients (r^2) and the slopes are presented at the bottom of the table. No symbol: not significant.

* $p < 0.05$.
** $p < 0.01$.
*** $p < 0.001$.

as well as potencies and efficacies of partial agonists and inverse agonists would have occurred. This, however, was not the case. In contrast, the behaviour of ligands, e.g. impentamine or imoproxifan, at one H_3R species homolog often opposed each other, against every expectation. Thus, these ligand effects are solely species-specific and not due to differences in constitutive activity of hH_3R and rH_3R.

3.5. [^{3}H]NAMH binding studies at hH_3R and rH_3R

Since the type of G protein co-expressed did not change the pharmacology of ligands at both hH_3R and rH_3R in the steady-state GTPase assay, we performed radioligand binding experiments for a further characterization only at membranes expressing hH_3R or rH_3R plus $G\alpha_{i2}$ plus $\beta_1\gamma_2$ dimers.

At first, we addressed the formation of a high-affinity ternary complex between the agonist [^{3}H]NAMH, the hH_3R or rH_3R and nucleotide-free G protein in saturation binding experiments (Fig. 5C and D). The K_d of [^{3}H]NAMH at hH_3R was 0.62 ± 0.21 nM, and the B_{max} was 0.62 ± 0.02 pmol/mg (n = 3). At rH_3R, the K_d value was 1.37 ± 0.36 nM, and the B_{max} was 0.48 ± 0.03 pmol/mg (n = 3). Interestingly, binding of [^{3}H]NAMH was only slightly GTPγS-sensitive in both cases. The K_d values of [^{3}H]NAMH in the presence of GTPγS (10 μM) were about 2-fold lower, but the B_{max} values did not change significantly (Fig. 5C and D).

In competition binding experiments (Fig. 4C), histamine (**1**) (Fig. 5E and F), N^{α}-methylhistamine (**2**), (*R*)-α-methylhistamine (**3**), imetit (**4**) and proxifan (**5**) had essentially the same affinities at hH_3R and rH_3R. Impentamine (**6**), imoproxifan (**7**) (Fig. 5E and F), ciproxifan (**8**) and thioperamide (**10**) (Fig. 5E and F) bound with higher affinity to rH_3R. Clobenpropit (**9**) also bound with similar affinity to both receptors. The pharmacological profiles, determined in [^{3}H]NAMH competition binding (Table 4) and steady-state GTPase assays (Table 3), compared with the literature, were very similar [31,32]. The pK_i and pEC_{50} values determined at hH_3R correlated well, suggesting a direct signal transfer in the Sf9 cell system (Fig. 7). However, at rH_3R, the correlation coefficient was rather low, due to an extraordinary high affinity of impentamine (**6**). Interestingly, the pK_i values of imoproxifan (**7**) were significantly lower than the corresponding pEC_{50} values determined in the GTPase assay (t test, $p < 0.05$).

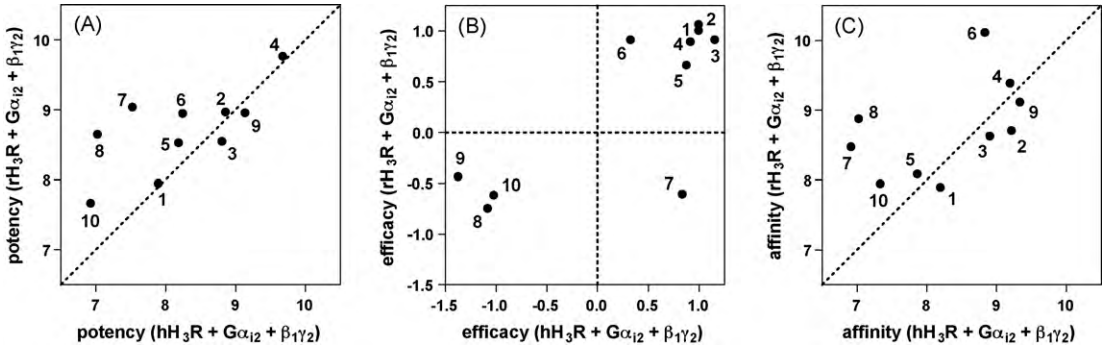

Fig. 4. Comparison of the pharmacological properties of hH_3R and rH_3R. (A) Comparison of the potencies of ligands in the GTPase assay. Data for hH_3R were taken from Ref. 23, data for rH_3R were taken from Table 3. (B) Comparison of the efficacies of ligands in the GTPase assay. Data for hH_3R were taken from Ref. [23], data for rH_3R were taken from Table 3. (C) Comparison of the affinities of ligands in the [^{3}H]NAMH competition binding assay. Data were taken from Table 4.

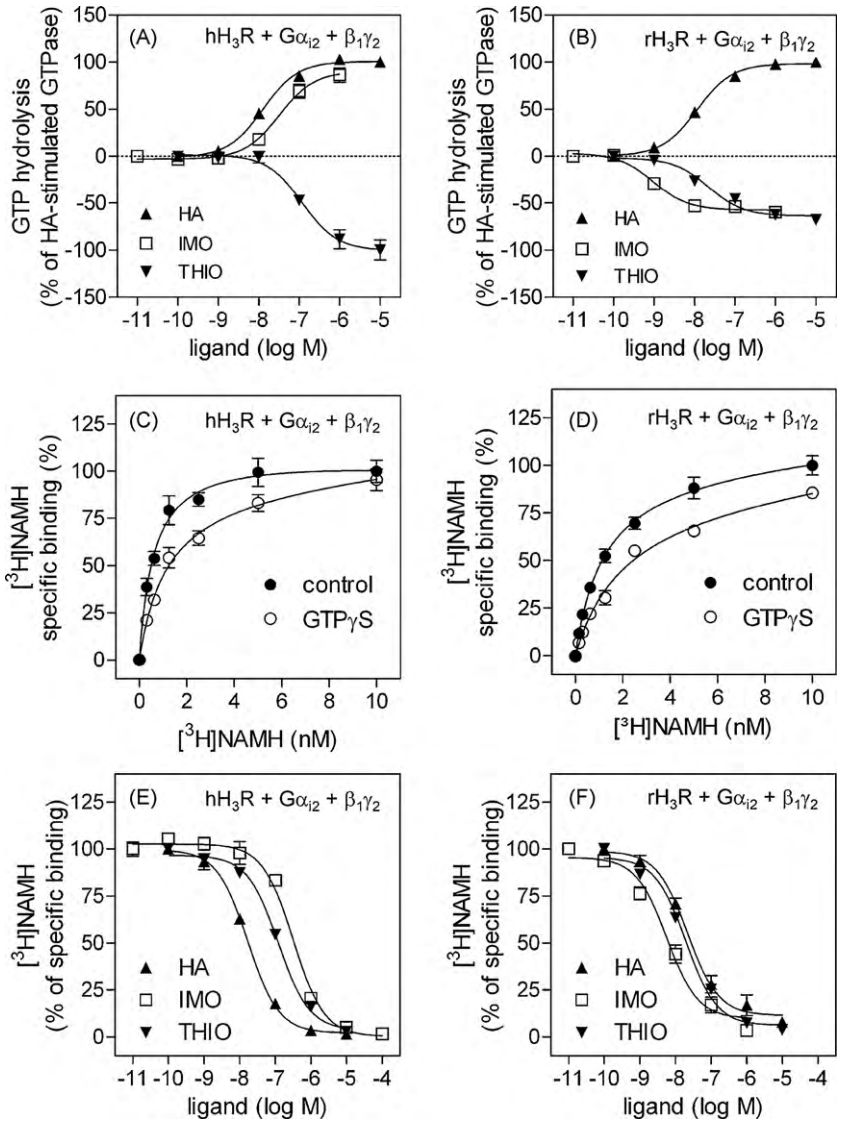

Fig. 5. Comparison of the effects of histamine, imoproxifan and thioperamide in membranes co-expressing the hH_3R or rH_3R, $G\alpha_{i2}$ subunits and $\beta_1\gamma_2$ dimers. (A and B) Steady-state GTPase activity in Sf9 membranes was determined as described under Section 2. Reaction mixtures contained HA, IMO or THIO at the concentrations indicated on the abscissa to achieve saturation. Data are expressed as percentage change in GTPase activity induced by the ligands compared to the GTPase activity stimulated by HA (10 μM), which was defined to be 100%. Data were analyzed by nonlinear regression and were best fit to sigmoidal concentration/response curves. Data points shown are the means ± S.E.M. of 3–4 independent experiments performed in duplicate. A summary of all results is shown in Table 3. (C and D) [^{3}H]NAMH saturation binding experiments were performed as described under Section 2. Data were analyzed by nonlinear regression and were best fitted to hyperbolic one-site saturation isotherms. The closed circles (●) show the data for the specific [^{3}H]NAMH binding in the absence of GTPγS (10 μM), the open circles (○) in the presence of GTPγS (10 μM). In (C), hH_3R was analyzed and in (D), rH_3R was analyzed. Data points shown are the means ± S.E.M. of 3 independent experiments performed in triplicate, using three different membrane preparations. (E and F) [^{3}H]NAMH binding was determined as described under Section 2. Reaction mixtures contained Sf9 membranes (10–50 μg of protein per tube) expressing the recombinant proteins, 1 nM [^{3}H]NAMH, and ligands at the concentrations indicated on the abscissa. (E) Competition binding at hH_3R and (F) competition binding at rH_3R. Data were analyzed for best fit to monophasic competition curves (*F* test). Data points shown are the means ± S.E.M. of 3–5 independent experiments performed in duplicate.

3.6. Binding mode of imoproxifan at hH_3R and rH_3R

To understand the molecular basis for the unique behaviour of imoproxifan, we performed molecular modelling studies with hH_3R and rH_3R. The binding modes of imoproxifan at active hH_3R and inactive rH_3R, representing the most favoured ligand–receptor complexes, are presented in Fig. 8.

Imoproxifan is bound to hH_3R and rH_3R in *E*-configuration, representing the *trans*-isomer of the oxime-moiety. The *E*-configuration was also determined to be the favoured one by crystallographic studies [33]. The electrostatic surface potential of the amino acids with the ligand in the binding pocket is shown (Fig. 8A and B). In hH_3R and rH_3R, the positively charged terminal imidazole moiety of imoproxifan interacts with the highly conserved $Asp^{3.32}$ (Fig. 8A and B, black arrow). However, there are large differences in electrostatic surface between TM V and TM III (Fig. 8A and B, yellow, dotted line). In this region, the electrostatic surface potential is positive in hH_3R due to the NH moiety of $Trp^{6.48}$, The analogous region in rH_3R shows a slightly negative potential due to the OH moiety of $Thr^{6.52}$. The consequence is a different orientation, and thus a different hydrogen bond networking of the oxime moiety of imoproxifan. In hH_3R, the methyl moiety points into direction of TM V, whereas in rH_3R, the methyl moiety points downward.

The reason for the differences in electrostatic surface potential between hH_3R and rH_3R are explained by the amino acid difference at position 3.37 between hH_3R and rH_3R. In hH_3R, $Glu^{5.46}$ can electrostatically interact with $Thr^{3.37}$ (Fig. 8C, yellow, dotted line).

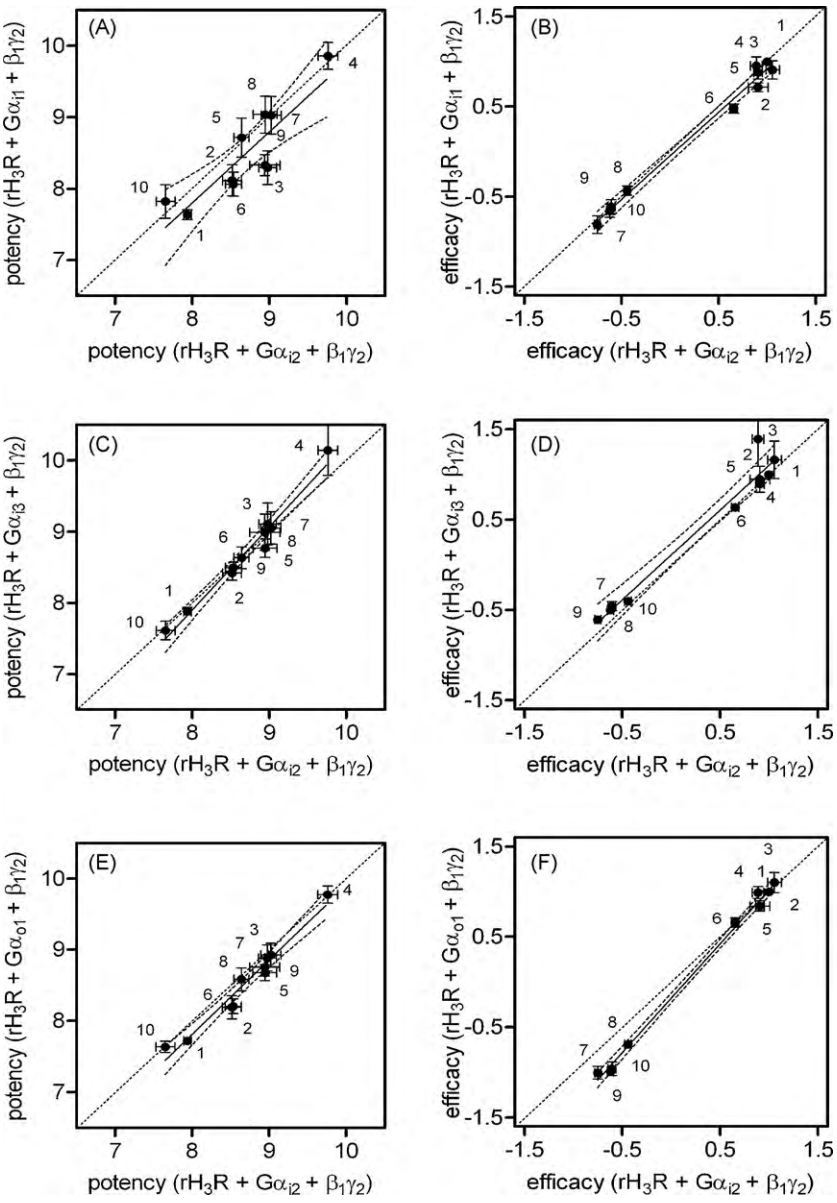

Fig. 6. Correlation of potency and efficacy of ligands at the rH_3R in the presence of different co-expressed $G\alpha_{i/o}$-proteins. Data shown in Table 3 were analyzed by linear regression. Numbers designate individual ligands decoded in Fig. 2. In (A), (C), and (E), the potencies of ligands at membranes co-expressing the rH_3R, $G\alpha_{i1}$, $G\alpha_{i3}$ or $G\alpha_{o1}$, and $\beta_1\gamma_2$-dimers, respectively, were correlated with values determined at the reference membrane expressing $G\alpha_{i2}$. (A) $r^2 = 0.77$; slope = 0.99 ± 0.19. (C) $r^2 = 0.97$; slope = 1.17 ± 0.07. (E) $r^2 = 0.96$; slope = 1.05 ± 0.07. In (B), (D) and (F), the efficacies of ligands at membranes co-expressing the rH_3R, $G\alpha_{i1}$, $G\alpha_{i3}$ or $G\alpha_{o1}$, and $\beta_1\gamma_2$ dimers, respectively, were correlated with values determined at the reference membrane expressing $G\alpha_{i2}$. (B) $r^2 = 0.99$; slope = 0.97 ± 0.04. (D) $r^2 = 0.96$; slope = 0.99 ± 0.07. (F) $r^2 = 0.996$; slope = 1.20 ± 0.03. The dotted lines indicate the 95% confidence intervals of the regression lines. The diagonal dashed line has a slope of 1 and represents a theoretical curve for identical values.

Thus, $Glu^{5.46}$ points towards $Thr^{3.37}$ and away from the binding pocket. Consequently, the electrostatic potential surface in this region is neutral and a small pocket for the methyl moiety of imoproxifan is build. In contrast, in rH_3R, $Thr^{3.37}$ is exchanged into $Ala^{3.37}$. Thus, an electrostatic interaction between $Glu^{5.46}$ and the amino acid side chain in position 3.37 is no longer possible. Instead, the modelling studies revealed an electrostatic interaction of $Glu^{5.46}$ and $Tyr^{3.33}$ in rH_3R (Fig. 8D, yellow, dotted line). Consequently, the negatively charged side chain of $Glu^{5.46}$ points partially toward the binding pocket, resulting in an aromatic contact between $Tyr^{3.33}$ and the imoproxifan.

A second species-difference between hH_3R and rH_3R near to the binding pocket is located at position 3.40. There is an alanine in hH_3R, but a bulkier valine in rH_3R (Fig. 8C and D, green, dotted line). It is likely that this amino acid difference also directs the oxime moiety of imoproxifan into a distinct orientation. Since $Ala^{3.40}$ is not as bulky as $Val^{3.40}$, there is more space for the oxime moiety to point downward in direction to 3.40 in hH_3R, than in rH_3R.

Additionally, $Trp^{6.48}$ is shown in its active conformation at hH_3R (Fig. 8C, blue arrow) and in its inactive conformation in rH_3R (Fig. 8D, blue arrow). $Trp^{6.48}$ is part of a highly conserved motif among GPCRs, thought to function as a toggle-switch during receptor activation, as is evident due to structural and biophysical studies [34]. $Trp^{6.48}$ horizontal to the membrane surface stabilizes the active state of a GPCR. $Trp^{6.48}$ vertical to the membrane surface stabilizes the inactive state of a GPCR. As consequence of the different amino acids at position 3.37 and 3.40 between hH_3R and rH_3R, the oxime moiety of imoproxifan can establish a hydrogen bond interaction to $Trp^{6.48}$ in its active conformation, thus stabilizing the active conformation of hH_3R

Table 4
[^{3}H]NAMH competition bindings in Sf9 membranes expressing hH_3R or rH_3R in combination with $G\alpha_{i2}$ and $\beta_1\gamma_2$.

	$pK_i \pm$ S.E.M.	
	$hH_3R + G\alpha_{i2} + \beta_1\gamma_2$	$rH_3R + G\alpha_{i2} + \beta_1\gamma_2$
HA	8.20 ± 0.04	7.89 ± 0.07
NAMH	9.22 ± 0.03	8.70 ± 0.09
RAMH	8.91 ± 0.07	8.62 ± 0.07
IME	9.20 ± 0.05	9.38 ± 0.08
PRO	7.87 ± 0.07	8.08 ± 0.10
IMP	8.84 ± 0.06	10.11 ± 0.05
IMO	6.92 ± 0.06	8.47 ± 0.09
CIP	7.03 ± 0.12	8.87 ± 0.08
CLOB	9.34 ± 0.06	9.11 ± 0.06
THIO	7.34 ± 0.04	7.94 ± 0.04
r^2 (pK_i/pEC_{50})	0.83	0.50
Slope (pK_i/pEC_{50})	0.94 ± 0.15	0.83 ± 0.29

Experiments were performed as described under Section 2. Reaction mixtures contained Sf9 membranes (10–50 μg of protein), 1 nM [^{3}H]NAMH, and unlabeled ligands at concentrations of 0.1 nM to 10 μM as appropriate to generate saturated competition curves. Data were analyzed by nonlinear regression and were best fit to one-site (monophasic) competition curves. Data shown are the means ± S.E.M. of 3–5 independent experiments performed in duplicate at 3 different membrane preparations. Additionally, data shown were correlated and analyzed by linear regression. The affinities and potencies of ligands at membranes co-expressing the hH_3R or rH_3R plus $G\alpha_{i2}$ plus $\beta_1\gamma_2$ dimers, respectively, were correlated. The correlation coefficients (r^2) and the slopes of all tested ligands are presented at the bottom of the table.

(Fig. 8E, yellow, dotted line). This interaction was not found in rH_3R. Here, the hydrogen of the oxime moiety interacts electrostatically with a negatively charged surface established by Thr$^{6.52}$ (Fig. 8F, yellow, dotted line). In rH_3R, the methyl group of imoproxifan is located in a small pocket established by Val$^{3.40}$ and Trp$^{6.48}$ in its inactive conformation.

Collectively, the different binding modes of imoproxifan in hH_3R and rH_3R presumably lead to differences in efficacies due to a different orientation of the oxime moiety and thus, stabilization of Trp$^{6.48}$ either horizontal or vertical to the membrane surface.

In contrast to imoproxifan (**7**), ciproxifan (**8**) (Fig. 4B) was found to act as an inverse agonist at hH_3R as well as at rH_3R. This observation is quite interesting, since both compounds only differ in the substitution pattern at the phenyl moiety (Fig. 2). To obtain more insight into these pharmacological differences, we docked ciproxifan (**8**) into the binding pocket of the active conformation of hH_3R and performed a minimization with regard to potential energy. An overlay with the corresponding imoproxifan–hH_3R complex showed, that the cyclopropyl moiety of ciproxifan (**8**), which is more space-filling than the methyl moiety of imoproxifan (**7**), lead to a shift of the neighbouring Glu$^{5.46}$ away from the binding pocket. Subsequently, the hydrogen bond between Glu$^{5.46}$ and Thr$^{3.37}$ is broken, which may lead to a destabilization of the entire ligand–receptor complex. In contrast, ciproxifan (**8**) could be docked very well into the binding pocket of the inactive hH_3R. The resulting binding mode is similar to that of imoproxifan (**7**) at the inactive rH_3R. Since there is the smaller alanine in position 3.40 at hH_3R (compared to valine at rH_3R), the more space-filling cycloproyl moiety fits optimally into this small pocket at hH_3R. However, the exchange of the oxime moiety into a carbonyl moiety in ciproxifan (**8**) leads to the loss of one hydrogen bond between ligand and receptor, as found for imoproxifan (Fig. 8F).

4. Discussion

Ligand pharmacology at hH_3R and rH_3R is species-dependent (Fig. 4) [35,36]. Unexpectedly, the species-differences can even span from agonism to inverse agonism in the case of imoproxifan [36]. In this study, we unraveled the underlying molecular mechanism of this reversal in efficacy. In steady-state GTPase assays, imoproxifan was an inverse agonist at rH_3R, but almost full agonist at hH_3R. Competition binding studies with [^{3}H]NAMH confirmed that the effect was receptor-mediated. Both hH_3R and rH_3R were expressed at similar levels and defined receptor-to-G protein stoichiometries. The basal activity in the two systems was comparable, as indicated by the similar inhibitory effects of the standard inverse agonist thioperamide. Thus, the unexpected behaviour of imoproxifan can only be due to species-specific differences in ligand recognition and receptor activation. Previous modelling studies described the binding mode of FUB181, a compound, similar to imoproxifan [21]. The orientation of imoproxifan in the binding pocket of H_3R, determined in the present study, is similar to these previous findings. In another study, it was suggested, that the Ala$^{3.40}$Val amino acid difference between hH_3R and rH_3R is responsible for the observed species-differences in antagonist pharmacology [13]. It was pointed out that thioperamide or compound A-304121 are in closer contact to Val$^{3.40}$ in rH_3R, than to Ala$^{3.40}$ in hH_3R. We could reproduce this finding because the affinity and potency of thioperamide was higher at rH_3R than hH_3R in our experimental system, too. Our molecular modelling studies further revealed that both amino acid differences in TM III, at position 3.37 and 3.40, are responsible for the differences in pharmacology of imoproxifan between hH_3R and rH_3R. The oxime moiety points downward in direction of Ala$^{3.40}$ in hH_3R. Thus, the polar oxime moiety is able to establish a hydrogen bond interaction with Trp$^{6.48}$ in its active conformation. In contrast, in rH_3R, the oxime moiety points toward TM V. Additionally, the methyl moiety of imoproxifan fits optimally into a small pocket between the bulky Val$^{3.40}$ and Trp$^{6.48}$ in its inactive conformation. The highly conserved Trp$^{6.48}$ is suggested to act as a

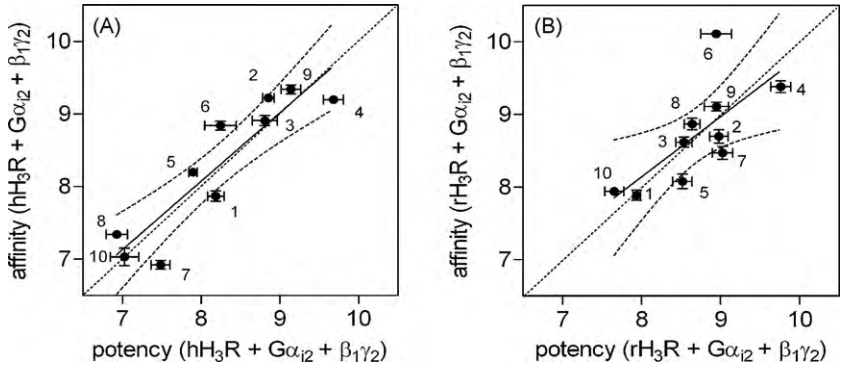

Fig. 7. Correlation of affinity and potency of ligands at the hH_3R and rH_3R. Data shown were analyzed by linear regression. Numbers designate individual ligands decoded in Fig. 2. In (A), the affinities and potencies of ligands at membranes co-expressing the hH_3R, $G\alpha_{i2}$ and $\beta_1\gamma_2$ dimers were correlated. (A) r^2 = 0.83; slope = 0.94 ± 0.15. In (B), the affinities and potencies of ligands at membranes co-expressing the rH_3R, $G\alpha_{i2}$ and $\beta_1\gamma_2$ dimers were correlated. (B) r^2 = 0.50; slope = 0.83 ± 0.29. The dotted lines indicate the 95% confidence intervals of the regression lines. The diagonal dashed line has a slope of 1 and represents a theoretical curve for identical values.

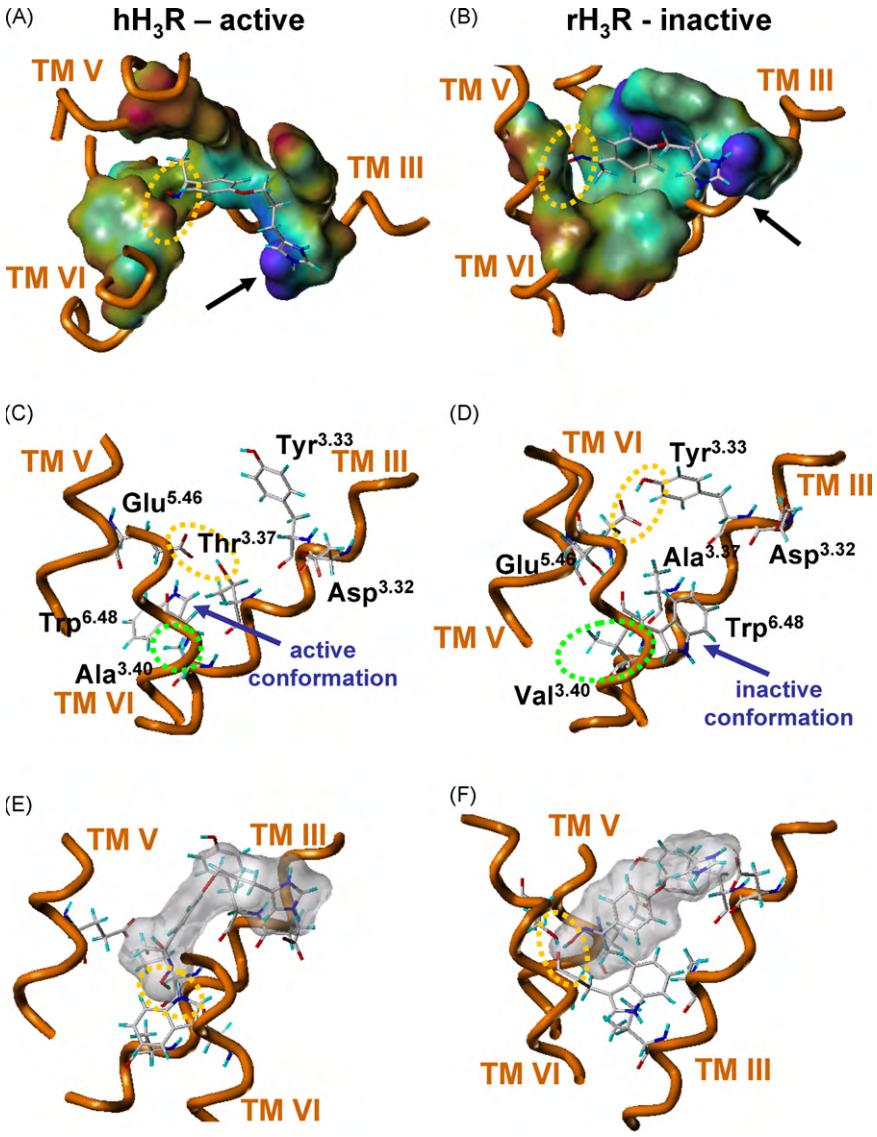

Fig. 8. Binding mode of imoproxifan at the active hH_3R and inactive rH_3R. (A) Electrostatic potential surface in the binding pocket of active hH_3R with imoproxifan in its binding conformation. (B) Electrostatic potential surface in the binding pocket of the inactive rH_3R with imoproxifan in its binding conformation. (A and B) Yellow dotted circle: the electrostatic potential is rather positive at hH_3R due to the NH moiety of $Trp^{6.48}$, but slightly negatively charged in rH_3R due to the OH moiety of $Thr^{6.52}$. The consequence is a different orientation of the ligands oxime moiety. (C) Conformation of amino acids in the imoproxifan bound state of active hH_3R. (D) Conformation of amino acids in the imoproxifan bound state of inactive rH_3R. (C and D) Yellow dotted circle: important differences in side chain conformation of $Glu^{5.46}$ between hH_3R and rH_3R. At hH_3R, $Glu^{5.46}$ interacts with $Thr^{3.37}$ and points away from the binding pocket. In rH_3R, $Thr^{3.37}$ is exchanged to $Ala^{3.37}$. Thus, the interaction between $Glu^{5.46}$ and the amino acid in position 3.37 is no longer possible and $Glu^{5.46}$ interacts with $Tyr^{3.33}$. Green dotted circle: in position 3.40, there is a small Ala in hH_3R, but the more bulky Val at rH_3R. It is suggested that this species difference is also be important for the different orientations of the oxime moiety between hH_3R and rH_3R. (E) Interaction between imoproxifan and hH_3R; (F) interaction between imoproxifan and rH_3R. (E and F) Yellow dotted circle: at hH_3R, the oxime moiety of imoproxifan points downwards and stabilizes the highly conserved $Trp^{6.48}$ in its active conformation by a hydrogen bond; at rH_3R, the oxime moiety of imoproxifan points upwards to TM V and interacts with $Thr^{6.52}$.

switch for receptor activation within biogenic amine receptors. $Trp^{6.48}$ oriented horizontally to the membrane surface is thought to stabilize the active state of a receptor, while $Trp^{6.48}$ oriented vertically to the membrane surface stabilizes the inactive state of a receptor. Since the hydrogen bond interaction between the oxime moiety and $Trp^{6.48}$ stabilizes $Trp^{6.48}$ in its active conformation in hH_3R, the partial agonism of imoproxifan is explained on a molecular level. This hydrogen bond-supported stabilization of $Trp^{6.48}$ in its active conformation is not possible in rH_3R. Here, in contrast to hH_3R, the methyl group near $Val^{3.40}$ and $Trp^{6.48}$ stabilizes $Trp^{6.48}$ in its inactive conformation due to a hydrophobic interaction. Thus, the modelling studies provide an explanation for the inverse agonism of imoproxifan at rH_3R on a molecular level, too. Additionally, the molecular modelling studies could be used to explain the switch from partial agonism of imoproxifan (**7**) to inverse agonism of ciproxifan (**8**) at hH_3R. The modelling studies suggest that the main reason for this is the more space-filling cycloproyl moiety of ciproxifan (**8**), compared to the methyl moiety in imoproxifan (**7**). This leads to a loss of hydrogen bonding between $Glu^{5.46}$ and $Thr^{3.37}$. Furthermore, a hydrogen bond between the carbonyl moiety and the NH moiety of $Trp^{6.48}$, stabilizing the active conformation of hH_3R, could not be established.

Interestingly, the pK_i values imoproxifan (**7**) at hH_3R and rH_3R were significantly higher than their pEC_{50} values (*t* test, $p < 0.05$). These results suggest that hH_3R and rH_3R can exist in a state of low partial agonist/inverse agonist affinity that interacts efficiently with G proteins. Another study, analyzing the hH_3R expressed in SK-N-MC cells by [^{3}H]NAMH competition binding and CRE-β-galactosidase reporter gene assays, revealed similar disparities

[31]. Similar results were also obtained when the human formyl peptide receptor, coupled to various G_i-proteins, was studied in Sf9 cell membranes [37]. In this study, the K_d of the agonist radioligand [^{3}H]fMLP was ~100-fold lower than the EC_{50} determined in GTPase experiments. Interestingly, at hH_3R expressed in Sf9 cells the low affinity state stabilized by imoproxifan (**7**) leads to an activation of G proteins, whereas in rH_3R, the low affinity state inhibited the activation of G proteins.

The G protein coupling profile of hH_3R and rH_3R was similar, too (Table 2; in [23]). An important fact is that like for hH_3R [23], at rH_3R no evidence for functional selectivity was observed (Table 3). However, in another study, evidence for functional selectivity at H_3R could be obtained [38]. Possible reasons for those discrepancies were already previously discussed [23]. Both hH_3R and rH_3R coupled effectively with G_i/G_o-proteins in Sf9 cell membranes, as was shown by GTPγS-insensitive ternary complex formation, using [^{3}H]NAMH as radioligand, and steady-state [γ-^{32}P]GTP hydrolysis. The similarly small shifts of the [^{3}H]NAMH saturation binding curves at hH_3R and rH_3R by GTPγS indicate a similarly strong interaction of both receptors with the G protein and are in line with the high constitutive activity of the H_3Rs. Thus, the results confirm the data of the GTPase experiments. In line with the data for hH_3R and rH_3R, high-affinity agonist binding to the structurally closely related histamine H_4-receptor is also largely GTPγS-insensitive [39]. The H_4-receptor possesses very high constitutive activity as well. Similar constitutive activity renders the system well suited for the analysis of species-specific ligand effects, since differences in constitutive activity between GPCRs can alter their pharmacological profiles and lead to a further complication of data interpretation [40,41].

The pharmacology of all histamine receptors (H_xRs) is species-dependent. This is especially true for H_xR agonists. At the H_1R, several classes of bulky ligands exhibit species differences [42]. Some of them show unique behaviours, like epimeric members of the ergoline family or chiral histaprodifens, switching from silent antagonism to partial agonism depending on the species studied [28,43]. Detailed molecular studies dissected some of the underlying mechanisms [26,44]. At the H_2R, bulky agonists like the long-chained impromidine- and arpromidine-derived guanidines or N^G-acylated imidazolylpropylguanidines (AIPGs), are more potent and efficacious at the gpH_2R than at the hH_2R [37,45]. Metiamide was identified to be an inverse agonist at the hH_2R, gpH_2R and rH_2R, but a weak partial agonist at the cH_2R [40]. At the H_4R, which has the lowest sequence similarity between species, studies focusing on ligand–receptor interactions of agonists are beginning to emerge [27,46]. However, the species-differences of imoproxifan at hH_3R and rH_3R described in this study represent the most substantial differences in pharmacology among H_XRs identified so far. This is particularly compelling in view of the fact that hH_3R and rH_3R sequences display a high degree of homology and only two amino acid residues cause the disparities.

In conclusion, we have shown that hH_3R and rH_3R expressed in Sf9 cells both similarly couple to defined G_i/G_o-protein heterotrimers and display similar constitutive activities. We show species-differences in pharmacological properties of imoproxifan and offer an explanation on the molecular basis for these differences. Most importantly, we introduce novel active state models of hH_3R and rH_3R that are suitable to explain the efficacy of H_3R ligands.

Acknowledgements

We would like to thank Mrs. G. Wilberg and Mrs. A. Seefeld for their excellent technical assistance. Thanks are also due to the reviewers for their helpful suggestions. This work was supported by the Research Training Program (Graduiertenkolleg) [GRK760] "Medicinal Chemistry: Molecular Recognition – Ligand–Receptor Interactions" of the German Research Foundation (DFG). The authors are affiliated with COST Action [BM0806].

References

[1] Hill SJ, Ganellin CR, Timmerman H, Schwartz JC, Shankley NP, Young JM, et al. International union of pharmacology. XIII. Classification of histamine receptors. Pharmacol Rev 1997;49:253–78.
[2] Leurs R, Bakker RA, Timmerman H, de Esch IJ. The histamine H3 receptor: from gene cloning to H3 receptor drugs. Nat Rev Drug Discov 2005;4:107–20.
[3] Leurs R, Chazot PL, Shenton FC, Lim HD, de Esch IJ. Molecular and biochemical pharmacology of the histamine H_4 receptor. Br J Pharmacol 2009;157:14–23.
[4] Zampeli E, Tiligada E. The role of histamine H_4 receptor in immune and inflammatory disorders. Br J Pharmacol 2009;157:24–33.
[5] Tiligada E, Zampeli E, Sander K, Stark H. Histamine H_3 and H_4 receptors as novel drug targets. Expert Opin Investig Drugs 2009;18:1519–31.
[6] Bongers G, Bakker RA, Leurs R. Molecular aspects of the histamine H_3 receptor. Biochem Pharmacol 2007;73:1195–204.
[7] Arrang JM, Morisset S, Gbahou F. Constitutive activity of the histamine H_3 receptor. Trends Pharmacol Sci 2007;28:350–7.
[8] Morisset S, Rouleau A, Ligneau X, Gbahou F, Tardivel-Lacombe J, Stark H, et al. High constitutive activity of native H_3 receptors regulates histamine neurons in brain. Nature 2000;408:860–4.
[9] Ireland-Denny L, Parihar AS, Miller TR, Kang CH, Krueger KM, Esbenshade TA, et al. Species-related pharmacological heterogeneity of histamine H_3 receptors. Eur J Pharmacol 2001;433:141–50.
[10] Wulff BS, Hastrup S, Rimvall K. Characteristics of recombinantly expressed rat and human histamine H_3 receptors. Eur J Pharmacol 2002;453:33–41.
[11] Ballesteros JH, Weinstein H. Integrated methods for the construction of three dimensional models and computational probing of structure–function relations in G-protein coupled receptors. Methods Neurosci 1995;25:366–428.
[12] Uveges AJ, Kowal D, Zhang J, Spangler TB, Dunlop J, Semus S, et al. The role of transmembrane helix 5 in agonist binding to the human histamine H_3 receptor. J Pharmacol Exp Ther 2002;301:451–8.
[13] Yao BB, Hutchins CW, Carr TL, Cassar S, Masters JN, Bennani YL, et al. Molecular modeling and pharmacological analysis of species-related histamine H_3 receptor heterogeneity. Neuropharmacology 2003;44:773–86.
[14] Ligneau X, Morisset S, Tardivel-Lacombe J, Gbahou F, Ganellin CR, Stark H, et al. Distinct pharmacology of rat and human histamine H_3 receptors: role of two amino acids in the third transmembrane domain. Br J Pharmacol 2000;131:1247–50.
[15] Hancock AA, Esbenshade TA, Krueger KM, Yao BB. Genetic and pharmacological aspects of histamine H_3 receptor heterogeneity. Life Sci 2003;73:3043–72.
[16] Kobilka B, Schertler GF. New G-protein-coupled receptor crystal structures: insights and limitations. Trends Pharmacol Sci 2008;29:79–83.
[17] Rasmussen SG, Choi HJ, Rosenbaum DM, Kobilka TS, Thian FS, Edwards PC, et al. Crystal structure of the human β_2-adrenergic G-protein-coupled receptor. Nature 2007;450:383–7.
[18] Jaakola VP, Griffith MT, Hanson MA, Cherezov V, Chien EY, Lane JR, et al. The 2.6 Å crystal structure of a human A_{2A} adenosine receptor bound to an antagonist. Science 2008;322:1211–7.
[19] Park JH, Scheerer P, Hofmann KP, Choe HW, Ernst OP. Crystal structure of the ligand-free G-protein-coupled receptor opsin. Nature 2008;454:183–7.
[20] Stark H, Sippl W, Ligneau X, Arrang JM, Ganellin CR, Schwartz JC, et al. Different antagonist binding properties of human and rat histamine H_3 receptors. Bioorg Med Chem Lett 2001;11:951–4.
[21] Schlegel B, Laggner C, Meier R, Langer T, Schnell D, Seifert R, et al. Generation of a homology model of the human histamine H_3-receptor for ligand docking and pharmacophore-based screening. J Comput Aided Mol Des 2007;21:437–53.
[22] Rai BK, Tawa GJ, Katz AH, Humblet C. Modeling G protein-coupled receptors for structure-based drug discovery using low-frequency normal modes for refinement of homology models: application to H_3 antagonists. Proteins 2010;78:457–73.
[23] Schnell D, Burleigh K, Trick J, Seifert R. No evidence for functional selectivity of proxifan at the human histamine H_3-receptor coupled to defined G_i/G_o protein heterotrimers. J Pharmacol Exp Ther 2010;332:996–1005.
[24] Cherezov V, Rosenbaum DM, Hanson MA, Rasmussen SG, Thian FS, Kobilka TS, et al. High-resolution crystal structure of an engineered human β_2-adrenergic G protein-coupled receptor. Science 2007;318:1258–65.
[25] Strasser A, Wittmann HJ. Analysis of the activation mechanism of the guinea-pig Histamine H_1-receptor. J Comput Aided Mol Des 2007;21:499–509.
[26] Strasser A, Wittmann HJ, Seifert R. Ligand-specific contribution of the N terminus and E2-loop to pharmacological properties of the histamine H_1-receptor. J Pharmacol Exp Ther 2008;326:783–91.
[27] Igel P, Geyer R, Strasser A, Dove S, Seifert R, Buschauer A. Synthesis and structure–activity relationships of cyanoguanidine-type and structurally related histamine H_4 receptor agonists. J Med Chem 2009;52:6297–313.
[28] Strasser A, Striegl B, Wittmann HJ, Seifert R. Pharmacological profile of histaprodifens at four recombinant histamine H_1-receptor species isoforms. J Pharmacol Exp Ther 2008;324:60–71.
[29] van der Spoel D, Lindahl E, Hess B, Groenhof G, Mark AE, Berendsen HJC. GROMACS: fast, flexible, and free. J Comput Chem 2005;26:1701–18.

[30] Thompson JD, Higgins DG, Gibson TJ. CLUSTAL W: improving the sensitivity of progressive multiple sequence alignment through sequence weighting, position-specific gap penalties and weight matrix choice. Nucleic Acids Res 1994;22:4673–80.
[31] Lim HD, van Rijn RM, Ling P, Bakker RA, Thurmond RL, Leurs R. Evaluation of histamine H_1-, H_2-, and H_3-receptor ligands at the human histamine H_4 receptor: identification of 4-methylhistamine as the first potent and selective H_4 receptor agonist. J Pharmacol Exp Ther 2005;314:1310–21.
[32] Bongers G, Krueger KM, Miller TR, Baranowski JL, Estvander BR, Witte DG, et al. An 80-amino acid deletion in the third intracellular loop of a naturally occurring human histamine H_3 isoform confers pharmacological differences and constitutive activity. J Pharmacol Exp Ther 2007;323:888–98.
[33] Sasse A, Sadek B, Ligneau X, Elz S, Pertz HH, Luger P, et al. New histamine H_3-receptor ligands of the proxifan series: imoproxifan and other selective antagonists with high oral *in vivo* potency. J Med Chem 2000;43:3335–43.
[34] Ahuja S, Smith SO. Multiple switches in G protein-coupled receptor activation. Trends Pharmacol Sci 2009;30:494–502.
[35] Lovenberg TW, Pyati J, Chang H, Wilson SJ, Erlander MG. Cloning of rat histamine H_3 receptor reveals distinct species pharmacological profiles. J Pharmacol Exp Ther 2000;293:771–8.
[36] Esbenshade TA, Estvander BR, Miller TR, Baranowski JL, Sharma R, Hancock AA, et al. Pharmacological classification of histamine H_3 receptor agents across species is attributable to transmembrane 3 sequence differences. Inflamm Res 2007;56(Suppl. 1):S45–6.
[37] Wenzel-Seifert K, Arthur JM, Liu HY, Seifert R. Quantitative analysis of formyl peptide receptor coupling to $G\alpha_{i1}$, $G\alpha_{i2}$, and $G\alpha_{i3}$. J Biol Chem 1999;274:33259–66.
[38] Krueger KM, Witte DG, Ireland-Denny L, Miller TR, Baranowski JL, Buckner S, et al. G protein-dependent pharmacology of histamine H_3 receptor ligands: evidence for heterogeneous active state receptor conformations. J Pharmacol Exp Ther 2005;314:271–8.
[39] Schneider EH, Schnell D, Papa D, Seifert R. High constitutive activity and a G-protein-independent high-affinity state of the human histamine H_4-receptor. Biochemistry 2009;48:1424–38.
[40] Preuss H, Ghorai P, Kraus A, Dove S, Buschauer A, Seifert R. Constitutive activity and ligand selectivity of human, guinea pig, rat, and canine histamine H_2 receptors. J Pharmacol Exp Ther 2007;321:983–95.
[41] Preuss H, Ghorai P, Kraus A, Dove S, Buschauer A, Seifert R. Mutations of Cys-17 and Ala-271 in the human histamine H_2 receptor determine the species selectivity of guanidine-type agonists and increase constitutive activity. J Pharmacol Exp Ther 2007;321:975–82.
[42] Seifert R, Wenzel-Seifert K, Bürckstümmer T, Pertz HH, Schunack W, Dove S, et al. Multiple differences in agonist and antagonist pharmacology between human and guinea pig histamine H_1-receptor. J Pharmacol Exp Ther 2003;305:1104–15.
[43] Pertz HH, Gornemann T, Schurad B, Seifert R, Strasser A. Striking differences of action of lisuride stereoisomers at histamine H_1 receptors. Naunyn Schmiedebergs Arch Pharmacol 2006;374:215–22.
[44] Strasser A, Wittmann HJ, Kunze M, Elz S, Seifert R. Molecular basis for the selective interaction of synthetic agonists with the human histamine H_1-receptor compared with the guinea pig H_1-receptor. Mol Pharmacol 2009;75:454–65.
[45] Kelley MT, Bürckstümmer T, Wenzel-Seifert K, Dove S, Buschauer A, Seifert R. Distinct interaction of human and guinea pig histamine H_2-receptor with guanidine-type agonists. Mol Pharmacol 2001;60:1210–25.
[46] Lim HD, Jongejan A, Bakker RA, Haaksma E, de Esch IJ, Leurs R. Phenylalanine 169 in the second extracellular loop of the human histamine H_4 receptor is responsible for the difference in agonist binding between human and mouse H_4 receptors. J Pharmacol Exp Ther 2008;327:88–96.